Millennial-scale glacial meltwater pulses and their effect on the spatiotemporal benthic δ^{18}O variability

T. Friedrich[1] and A. Timmermann[1]

Received 9 April 2012; revised 4 July 2012; accepted 6 July 2012; published 17 August 2012.

[1] Ratios of oxygen isotope values obtained from foraminiferal calcite are one of the most established paleoceanographic proxies. They are used in the context of estimating variations in ice volume, ocean temperature, and salinity and provide a means to date marine sediment cores across different ocean basins. Our study addresses the question how the δ^{18}O of the deglacial meltwater signal propagates into the interior ocean, when large-scale millennial-scale reorganizations of the Atlantic Meridional Overturning Circulation (AMOC) are present. Analyzing a series of idealized tracer-injection experiments conducted with an earth system model, we find that a substantial weakening of the AMOC leads to a massive delay in the export of the glacioeustatic oxygen isotope signal into the deep ocean, whereas the Atlantic-Pacific lag in benthic oxygen isotope signals is not increased. Furthermore, it is shown that an AMOC cessation causes a decoupling of δ^{18}O propagation time and water mass age, in particular in the deep Pacific. Our results lend further support to the notion that benthic oxygen isotope records obtained from stacks are not a useful global chronostratigraphic tool during periods of millennial-scale global ocean circulation changes. The regionally varying delay effect of the deglacial sea level signal studied here adds onto existing uncertainties in the interpretation and decomposition of benthic oxygen isotope in terms of sea level, temperature, and hydrographic variations.

Citation: Friedrich, T., and A. Timmermann (2012), Millennial-scale glacial meltwater pulses and their effect on the spatiotemporal benthic δ^{18}O variability, *Paleoceanography*, *27*, PA3215, doi:10.1029/2012PA002330.

1. Introduction

[2] Since the late 1960s oxygen isotopic records of planktonic and benthic foraminifera have been used to reconstruct paleo-temperatures [*Emiliani*, 1966] and ice volume changes [*Shackleton*, 1967]. δ^{18}O values [$\delta^{18}\mathrm{O} = \left(\frac{^{18}\mathrm{O}}{^{16}\mathrm{O}}\right)_{sample} \Big/ \left(\frac{^{18}\mathrm{O}}{^{16}\mathrm{O}}\right)_{standard} - 1) \times 1{,}000$] derived from planktonic or benthic calcite are a function of both the local temperature in which calcification occurred and the local isotopic composition of the ambient seawater. The latter can be altered by hydrographic changes (e.g. changes in the water mass distribution) and by changes in sea level. Thus, for benthic calcite $\delta^{18}\mathrm{O}_{b-cc}(\vec{x},t)$ we can decompose the spatio-temporal variability as

$$\delta^{18}\mathrm{O}_{b-cc}(\vec{x},t) = \delta^{18}\mathrm{O}_{sl}(\vec{x},t) + \delta^{18}\mathrm{O}_{temp}(\vec{x},t) + \delta^{18}\mathrm{O}_{hydro}(\vec{x},t), \quad (1)$$

with the terms on the right hand side of the equation representing the sea level component, the temperature-dependent fractionation component and the water mass (or hydrographic) component, respectively. Distinguishing between the sea level, local temperature and water mass contributions in any sediment-based δ^{18}O signal poses one of the major challenges in paleoceanography [*Waelbroeck et al.*, 2011]. The high degree of co-variability between these signals on glacial timescales further complicates the attribution.

[3] Note, that we have introduced a spatially dependent sea level contribution $\delta^{18}\mathrm{O}_{sl}(\vec{x},t)$. We further write $\delta^{18}\mathrm{O}_{sl}(\vec{x},t)$ as

$$\delta^{18}\mathrm{O}_{sl}(\vec{x},t) = 0.0072414 \ \frac{‰}{\mathrm{m}} \ \eta(t) + \delta^{18}\mathrm{O}'_{sl}(\vec{x},t), \quad (2)$$

where $\eta(t)$ captures the glacioeustatic global sea level anomalies in meters which is translated into a mean ocean δ^{18}O change through a factor of 1.05 ‰/145 m [*Waelbroeck et al.*, 2011]. The second term on the right hand side [$\delta^{18}\mathrm{O}'_{sl}(\vec{x},t)$] is the regional deviation from this global mean associated with the propagation of the ice volume δ^{18}O signal from the source to the core region. This regional term will depend on the circulation state, which, at least on millennial timescales, is heavily influenced by the deglacial freshwater forcing in the North Atlantic. The latter is related to the time derivative of η, abbreviated here as $\dot{\eta}(t)$.

[1]International Pacific Research Center, School of Ocean and Earth Sciences and Technology, University of Hawai'i at Mānoa, Honolulu, Hawaii, USA.

Corresponding author: T. Friedrich, International Pacific Research Center, School of Ocean and Earth Sciences and Technology, University of Hawai'i at Mānoa, 1680 East-West Rd., POST Bldg., Honolulu, HI 96822, USA. (tobiasf@hawaii.edu)

0883-8305/12/2012PA002330

[4] Symbolically we can hence write

$$\delta^{18}O_{b-cc}(\vec{x},t) = 0.0072414 \ \frac{[‰]}{m} \ \eta(t) + \delta^{18}O'_{sl}[\vec{x},\dot{\eta}(t)] + \delta^{18}O_{temp}[\vec{x},\dot{\eta}(t)] + \delta^{18}O_{hydro}[\vec{x},\dot{\eta}(t)]. \quad (3)$$

Older studies [*Shackleton*, 1967; *Broecker and van Donk*, 1970; *Shackleton and Opdyke*, 1973] have almost entirely attributed changes in benthic δ^{18}O to changes in glacioeustatic sea level. More recent studies [*Waelbroeck et al.*, 2002; *Skinner and Shackleton*, 2005] accounted for the contributions of temperature, regional sea level and hydrographic changes, but combined the regional sea level term $\delta^{18}O'_{sl}[\vec{x},\dot{\eta}(t)]$ and the hydrographic term $\delta^{18}O_{hydro}[\vec{x},\dot{\eta}(t)]$ in their analysis of deep ocean oxygen isotope budgets. The goal of our study is to provide a better understanding of the spatiotemporal behavior of $\delta^{18}O'_{sl}[\vec{x},\dot{\eta}(t)]$ and the dependence of the propagation time of a tracer, released into the North Atlantic, on the ocean circulation state and the deglacial freshwater forcing.

[5] Comparing benthic δ^{18}O records from the Atlantic and the Pacific, it has been argued that the Pacific δ^{18}O lags the Atlantic by 1,000–4,000 years during the last six terminations and that age models that are based on the alignment of benthic δ^{18}O are subject to an uncertainty of ~4,000 years [*Lisiecki and Raymo*, 2009]. It serves well to take a closer look at the underlying mechanisms and potential explanations.

[6] Recent modeling studies for instance [*Wunsch and Heimbach*, 2008; *Siberlin and Wunsch*, 2011] found a strong dependence of the equilibration time of passive tracers on the location of tracer injection as well as on other boundary conditions. Moreover, during glacial terminations reorganizations of the large-scale ocean circulation may have affected the spreading of the deglacial meltwater tracer signal into the interior ocean. As discussed above, this effect is captured by $\delta^{18}O'_{sl}[\vec{x},\dot{\eta}(t)]$. Both effects are likely to further limit the applicability of benthic δ^{18}O as a global chronostratigraphic correlation tool, at least on millennial timescales.

[7] One striking example of non-uniform benthic δ^{18}O variability is the apparent ~4,000 year lag between deglacial benthic δ^{18}O changes in the Pacific and Atlantic, reported by *Skinner and Shackleton* [2005]. The authors argued that deep water hydrographic variations can explain some of the heterogeneity seen in benthic oxygen isotope records in the Atlantic and Pacific. An alternative explanation was provided in *Gebbie* [2012]. Using a steady ocean circulation field he argued that various regional δ^{18}O injection scenarios can also reproduce the *Skinner and Shackleton* [2005] data. One of the key assumptions of *Gebbie* [2012] is that δ^{18}O is a strictly passive tracer that does not affect the ocean circulation. However, the deglacial δ^{18}O injection is inherently coupled to an equivalent freshwater forcing which is likely to affect the global ocean circulation and hence the propagation of the tracer in the deep ocean.

[8] In particular during Heinrich event 1 [*Hemming*, 2004] (~17–15 ka B.P.), freshwater forcing from melting icebergs, accompanied by a decrease in North Atlantic surface δ^{18}O (Figure 1b) has been suggested as the trigger for massive reorganizations of the ocean circulation in the North Atlantic and Pacific [*Vidal et al.*, 1997; *Bard et al.*, 2000; *Clark et al.*, 2002; *Elliot et al.*, 2002; *McManus et al.*, 2004; *Okazaki et al.*, 2010]. These circulation changes must have affected the propagation of the deglacial δ^{18}O signal with potential implications for the interpretation of inter-basin leads and lags. If δ^{18}O variations originated from deglacial meltwater changes, the doublet (δ^{18}O, salinity) would have to be treated as an active tracer, thereby challenging the use of empirically derived steady ocean state transit time distributions (TTD) [*Holzer and Hall*, 2000; *Peacock and Maltrud*, 2006] and total matrix intercomparisons [*Gebbie and Huybers*, 2010, 2011] in the context of rapidly occurring ice sheet variability.

[9] Using an earth system model of intermediate complexity we present a series of spatiotemporal solutions for the regionally varying sea level component of the deglacial δ^{18}O signal. In a first set of idealized experiments we apply constant δ^{18}O-tracer forcing to the surface of the North Atlantic. Different ocean circulation regimes are obtained by applying different freshwater forcing scenarios over the same region of the North Atlantic leading to temporary, substantial AMOC weakening. The constant δ^{18}O-forcing will allow for an assessment of the different propagation pathways and equilibration timescales for different circulation regimes. In a second set of experiments we derive a more realistic transient tracer forcing for the earth system model by combining paleoceanographic records of planktonic δ^{18}O from the North Atlantic. Capturing the deglacial evolution of the AMOC and the surface North Atlantic δ^{18}O signal due to disintegrating ice sheets, these experiments provide a more in-depth understanding of lead-lag relationships between different ocean basins with the aim to better understand the dynamics of $\delta^{18}O'_{sl}(\vec{x},t)$ and to estimate the contributions of temperature, sea level and water mass changes to benthic δ^{18}O variations in different marine sediment records.

[10] Our paper is organized as follows. In section 2 we describe the model configuration. The design of the perturbation experiments is outlined in section 3. Our main results will be presented and discussed in section 4. Section 5 provides a brief summary of our results and some conclusions.

2. Model Configuration

[11] We conducted a series of experiments using the atmosphere-ocean-sea ice-carbon cycle model LOVECLIM [*Goosse et al.*, 2010]. LOVECLIM is a well established model for paleo-climate simulations. It is based on the ECBilt-CLIO Earth system model of intermediate complexity extended by components for vegetation and the marine carbon cycle. The marine carbon cycle component has been deactivated for our study. LOVECLIM's sea ice-ocean component (CLIO) [*Goosse et al.*, 1999] is a primitive equation ocean model on z coordinates with a horizontal resolution of 3° × 3° and 20 levels in the vertical with thicknesses ranging from 10 m to ~700 m coupled to a thermodynamic-dynamic sea ice model. The horizontal advection of scalars and tracers is discretized by a hybrid scheme [*Rood*, 1987; *Campin*, 1997] which is based on a weighted upwind scheme and centered scheme. The weighting factor varies in space and time and is calculated according to *Campin* [1997]. Mixing along isopycnals, the effect of mesoscale eddies on transports and mixing as well as downsloping currents at the bottom of continental shelves are parameterized according to *Goosse et al.* [2010]. The strength of diapycnal mixing is coupled to the regionally

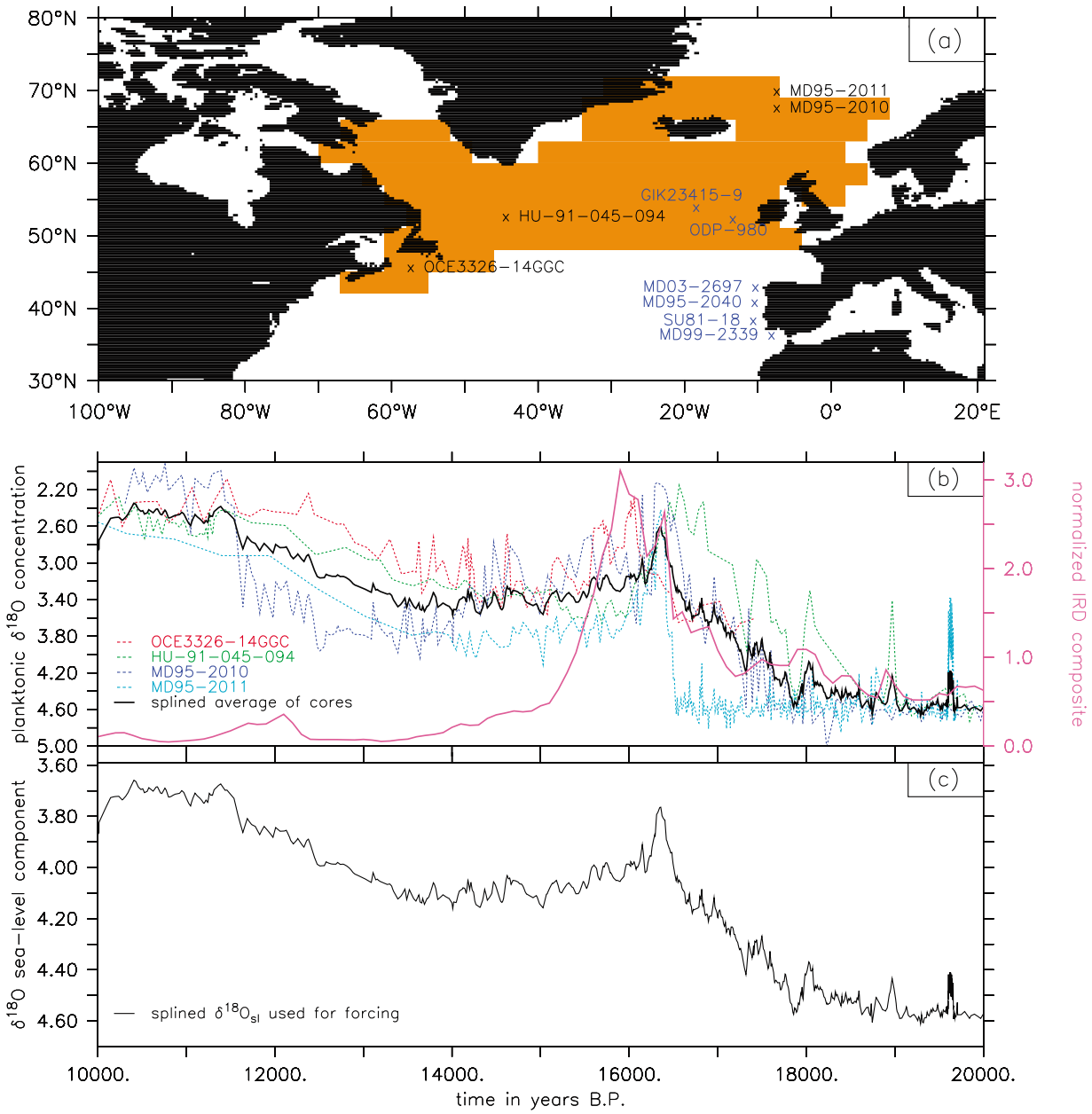

Figure 1. (a) Region of passive tracer (0–100 m) and freshwater (surface only) forcing for all simulations (see also Table 1). Locations of sediment cores used for transient forcing are indicated by black crosses. Blue crosses indicate location of sediment cores that were used for an IRD composite for comparison. (b) Planktonic δ^{18}O (splined) as recorded in the sediment cores and indicated in the panel. Black line represents splined average of core data. Pink line represents an splined IRD composite (normalized by individual standard deviations) of cores indicated by blue crosses in Figure 1a. (c) Normalized δ^{18}O average used for transient forcing. A sea level rise of 100 m between 20–10 ka B.P. was assumed [*Lambeck and Chappell*, 2001] equivalent to 0.7 permil δ^{18}O for scaling.

varying roughness of bottom topography [*Decloedt and Luther*, 2010] as described in detail in *Friedrich et al.* [2011]. In this newly developed mixing scheme it is assumed that the total topography-catalyzed mixing can be expressed in terms of the topographic roughness. The modified vertical background mixing scheme employed in our study has the functional form:

$$K[h, r(x,y)] = K_b(r)[1 + h/h_0(r)]^{-2} + K_0 \qquad (4)$$

where the boundary diffusivity $K_b(r)$ and decay scale $h_0(r)$ are simple functions of topographic roughness $r(x,y)$ that have been determined empirically from ~300 microstructure observations of turbulent kinetic energy dissipation rates [*Decloedt and Luther*, 2010]. The diffusivity $K_0 = 5.6 \times 10^{-6}$m^2/s is the minimum diffusivity that can be sustained by the Garret-Munk internal wavefield [*Polzin et al.*, 1995] assuming a mixing efficiency of C = 0.2. The topographic roughness $r(x,y)$ and $h_0(r)$ were derived from

Table 1. Abbreviation, Description, "δ^{18}O" Forcing and Freshwater (FW) Forcing for All Model Runs[a]

Model Run	Description	"δ^{18}O" Forcing	FW Forcing
CONST-CTR	control run to study equilibration timescale	constant	no FW forcing
CONST-FW1ka	equilibration timescale for ~2,000 years AMOC shutdown	constant	0.5 Sv for 1,000 years
CONST-FW2ka	equilibration timescale for ~3,000 years AMOC shutdown	constant	0.5 Sv for 2,000 years
CONST-noAMOC	equilibration timescale for very weak AMOC	constant	0.5 Sv for entire run
T1-CTR	control run to study propagation of δ^{18}O signal during Termination 1	δ^{18}O stack	no FW forcing
T1-H1	propagation of δ^{18}O including Heinrich event 1	δ^{18}O stack	0.5 Sv for 2,000 years

[a]The forcing for the passive tracer was applied over the first 100 m of the orange region depicted in Figure 1a. FW forcing was applied to the surface of the indicated region. The δ^{18}O data used for the time-varying forcing are shown in Figures 1b and 1c.

altimeter-derived seafloor topography of *Smith and Sandwell* [1997] with a resolution of 2 arc-minutes between 72°S–72°N. In order to incorporate the new vertical background mixing parametrization into ocean component CLIO, average diffusivities for each 3° × 3° grid cell were calculated.

[12] The atmosphere model (ECBilt) is a spectral model in T21 (~5.625° × 5.625°) resolution, based on quasi-geostrophic equations with 3 vertical levels. Ageostrophic forcing terms are estimated from the vertical motion field and added to the prognostic vorticity equation and thermodynamic equation. Diabatic heating due to radiative fluxes, the release of latent heat and the exchange of sensible heat with the surface are parameterized. The seasonally and spatially varying cloud cover climatology is prescribed in ECBilt. It should be noted that an interactive atmospheric component is crucial for the simulation of large-scale ocean circulation changes. The ocean, atmosphere and sea ice component of the ECBilt-CLIO model are coupled by exchange of momentum, heat and freshwater fluxes. The hydrological cycle over land is closed by a bucket model for soil moisture and simple river runoff scheme and a freshwater flux correction is applied to account for an underestimation of the Atlantic/Pacific moisture transport.

[13] Two additional passive tracers are active in CLIO: an artificial dye tracer to study the effects of ocean advection and mixing on the propagation of a deglacial $\delta^{18}O_{sl}(\vec{x},t)$ signal (details are given in the next section) and an age tracer. The idealized water mass age tracer is set to zero at the surface and attains values increasing in time, depending on advection, diffusion and convection in the system [*England*, 1995].

[14] Details on the performance of LOVECLIM under different climate conditions can be found in *Renssen et al.* [2002], *Justino et al.* [2005], *Menviel et al.* [2008], *Goosse et al.* [2010], and *Friedrich et al.* [2011].

3. Experiment Design

[15] Two different types of experiments were conducted using either a constant or a time-varying forcing for a purely passive tracer in the North Atlantic. In case of constant forcing a passive tracer is set to the arbitrary concentration of 1,000 over the first 100 m in the orange region shown in Figure 1a. Everywhere else the tracer is initialized with a concentration of zero. The concentration of 1,000 is strongly relaxed in the forcing region over the entire integration time and can evolve freely in the rest of the model domain. Since a prescribed concentration represents an infinite source, a concentration of 1,000 should eventually be reached at every grid cell through advection and mixing. Four sensitivity experiments were conducted to study the equilibration timescale of the passive tracer under different AMOC regimes (Figure 2a): The control run (CONST-CTR) uses no freshwater (FW) forcing. In three additional runs, FW-forcing was applied to the surface of the North Atlantic for 1,000 years (CONST-FW1ka), 2,000 years (CONST-FW2ka) or the entire integration time of 6,000 years (CONST-noAMOC) respectively. A summary of the model runs is given in Table 1. The FW-forcing amounts to 0.5 Sv and was applied as FW flux over the orange region indicated in Figure 1a. For the simulations CONST-FW1ka and CONST-FW2ka the initialization of the passive tracer and the FW-forcing started simultaneously. In case of the CONST-noAMOC run the FW-forcing started 600 years prior to the tracer initialization to allow for the spin-down of the AMOC.

[16] The transient experiments are designed to elucidate the propagation characteristics of the $\delta^{18}O_{sl}(\vec{x},t)$ signal during the Last Glacial Termination. The integrations cover the time period of 20–10 ka before present (B.P.).

[17] To derive a more realistic transient δ^{18}O forcing scenario that captures the effect of deglacial ice sheet melting we averaged and smoothed the planktonic δ^{18}O records of the northern North Atlantic sediment cores HU-91-045-094 [*de Vernal and Hillaire-Marcel*, 2000], OCE3326-14GGC [*Keigwin et al.*, 2005], MD-95-2010 [*Dokken and Jansen*, 1999] and MD-95-2011 [*Dreger*, 1999] (see Figure 1b). To generate a time-dependent δ^{18}O deglacial meltwater forcing signal for T1-CTR and T1-H1, the composite of the planktonic δ^{18}O records was scaled such that the volume average in our model between the LGM and 10 ka B.P. amounts to ~0.7 permil δ^{18}O-equivalent corresponding to ~100 m of deglacial sea level rise (see equation (2)) [*Lambeck and Chappell*, 2001].

[18] For the experiments TR-CTR and TR-H1 the upper ocean (100 m) tracer concentration in the orange forcing region (Figure 1a) is strongly relaxed to the remaining glacioeustatic δ^{18}O forcing signal (see Figure 1c). In the rest of the model domain the oxygen isotope tracer was initialized with the first value of the forcing time series and allowed to vary freely thereafter. This is a somewhat arbitrary procedure

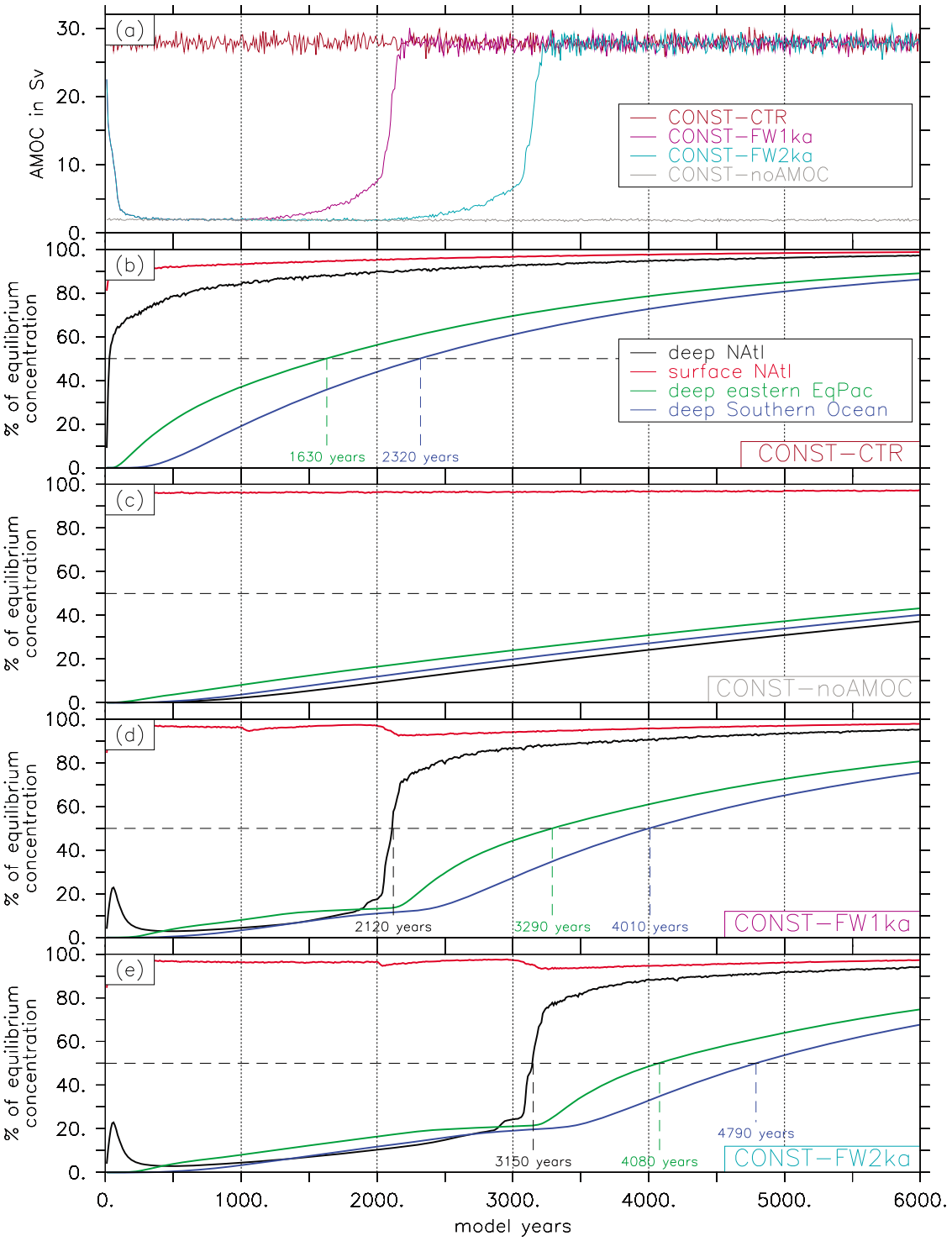

Figure 2. (a) AMOC in Sv for the different experiments as indicated in the panel. The strength of the AMOC is defined by the maximum of the overturning in the Atlantic north of 30°N. (b) Passive tracer concentration for CONST-CTR run in percent of equilibrium concentration averaged for deep (depth > 2,000 m, black) and surface (red) North Atlantic (75°W–30°E/45°N–70°N), deep Southern Ocean (blue, 45°S–80°S, depth > 2,000 m) and deep eastern Equatorial Pacific (green, 120°W–90°W/10°S–10°N, depth > 2,000 m). (c–e) Same as Figure 2b for experiments CONST-noAMOC, CONST-FW1ka and CONST-FW2ka, respectively. Basin-averages of half-saturation times are indicated by dashed lines and numbers in the panels.

as it removes any spatial δ^{18}O gradients which were shown to be in the order of 5 permil for a present-day ocean [*LeGrande and Schmidt*, 2006]. Furthermore it assigns planktonic δ^{18}O values also to regions that are regarded as benthic. However, as can be seen in *Skinner and Shackleton* [2005], benthic δ^{18}O concentrations have been virtually identical in the deep eastern equatorial Pacific and at the Iberian Margin around 20 ka ago. It was not our intention to provide a complete simulation of the deglacial δ^{18}O evolution. Our main goal is to examine the effects of ocean circulation changes on the propagation of the temporally evolving $\delta^{18}O_{sl}(\vec{x}, t)$ signal.

[19] The control simulation (T1-CTR, see Table 1) uses only the transient surface δ^{18}O forcing (Figure 1c) and the tracer is treated as a passive tracer. To account for the effects of large-scale changes in ocean circulation during H1 on the signal propagation, an experiment (T1-H1) was designed in which 0.5 Sv FW-forcing was applied for 2,000 years to generate a ~3,000 yearlong AMOC shutdown starting at 18 ka B.P., in qualitative agreement with reconstructions from the North Atlantic [*Bard et al.*, 2000; *Clark et al.*, 2002; *McManus et al.*, 2004]. It should be noted here that the idealized duration, strength and temporal evolution of the FW-forcing was chosen according to the AMOC sensitivity of the Earth system model. A value of 0.5 Sv applied over a period of 2,000 years corresponds to about 90 m sea level rise which is more than current estimates for H1 [*Siddall et al.*, 2003]. Furthermore, the rectangular shape of the forcing was chosen for simplicity. It proves very difficult to derive the exact North Atlantic FW-forcing from planktonic δ^{18}O data.

[20] All simulations were run under preindustrial boundary conditions but with a closed Bering Strait. The passive δ^{18}O tracer is subject to the exact same advection and mixing as temperature and salinity. Surface fluxes and temperature-dependency of δ^{18}O are not taken into account. The FW-hosing experiments were conducted without salinity compensation.

[21] Our study only considers North Atlantic injections of the deglacial δ^{18}O signal and ignores any potential contributions from Antarctica.

4. Results and Discussion

4.1. Constant Tracer-Forcing in the North Atlantic

[22] The control simulation (CONST-CTR) is characterized by a stable AMOC with a mean value of about 28 Sv (defined by the maximum of the overturning in the Atlantic north of 30°N) (Figure 2a). The strong overturning is partly generated by the closed Bering Strait which inhibits salinity exchange between the Arctic and the Pacific leading to a saltier North Atlantic [*Hu et al.*, 2010]. NADW production allows the artificial tracer to reach the deep North Atlantic within several years to decades (Figure 3a). From here it is exported along the NADW path in the deep western boundary current (Figures 4a and 4b) and is detectable in the Southern Ocean after about 100 years. The spreading into the Pacific and the Indian Ocean occurs mostly along the bottom water path. The North Pacific is reached through a slow process involving vertical mixing. Due to the distinct propagation path, local equilibration timescales are very different and do not necessarily reflect the distances to the source. The water column of the Atlantic north of 40°N and the Arctic Ocean becomes fully equilibrated after about 1,000 years (Figure 3b). By this time, tracer concentrations in the intermediate depth range of the North Pacific are still below 10% of the equilibrium concentration. After about 3,000 model years concentrations in the North Pacific are half equilibrated. The South Atlantic still exhibits a vertical gradient with lowest concentration at intermediate depths (see Figure 3c).

[23] The propagation pathway and ocean 'turn-over' timescale change dramatically when the AMOC is severely reduced. The permanent FW-forcing in the CONST-noAMOC experiment reduces the AMOC down to values of about 2 Sv (Figure 2a). As a consequence of a shutdown of NADW production, the artificial δ^{18}O tracer cannot reach the deeper layers of the North Atlantic (Figure 3e) and the deep western boundary current ceases to flow to the south (Figure 4e). The propagation occurs near the surface into the Southern Ocean and the Pacific (Figures 3f and 3g). Interestingly, upper layers of the North Pacific are reached faster in case of a weak North Atlantic overturning. After 1,000 years concentrations in the North Pacific in the depth range of 1,000 m are higher in case of AMOC cessation than for CONST-CTR (Figure 3g). The main reason is the corresponding large-scale circulation change in the North Pacific. As a result of the AMOC weakening, an overturning circulation develops in the North Pacific (PMOC) (Figure 3e), in good agreement with reconstructions for Heinrich event 1 and previous model results [*Okazaki et al.*, 2010]. As shown in Figure 3e, this PMOC reaches in our model values of about 15 Sv. It increases the influx of water into the North Pacific at the surface and enhances ventilation of the intermediate depth range of 800–2,000 m. In the long run, however, the equilibration timescales are dominated by the slow efflux of the tracer out of the North Atlantic. At the end of the integrations after 6,000 years, the artificial tracer concentrations are almost everywhere significantly lower in the CONST-noAMOC run compared to the control experiment (CONST-CTR) with the North Pacific not even reaching 50% of the saturation concentration (Figures 3d and 3h and Figures 2b and 2c).

[24] The experiments CONST-CTR and CONST-noAMOC can be regarded as the two extreme scenarios of our idealized simulation of the δ^{18}O tracer propagation. They provide valuable insight into the propagation characteristics that helps explain features of the simulations of temporary AMOC weakening in the experiments CONST-FW1ka and CONST-FW2ka. It takes the AMOC about 200 years in both simulations to drop to values of 2 Sv (Figure 2a). During this short time, while NADW formation is still active, a fraction of the tracer is transported into the deep North Atlantic leading to a temporary increase in the artificial tracer concentration (Figures 2d and 2e). After the complete cessation of AMOC transport the tracer supply to the deep North Atlantic is brought to a halt and North Atlantic concentrations decrease again due to the entrainment of waters low in tracer concentration. Until the AMOC resumes after about 2,000 and 3,000 years respectively, the evolution of the averaged tracer concentration in CONST-FW1ka and CONST-FW2ka resembles that of CONST-noAMOC. With the beginning AMOC recovery, a transition phase of a few hundred years can be identified after which the evolution of the our idealized δ^{18}O tracer concentration is similar to the CONST-CTR experiment.

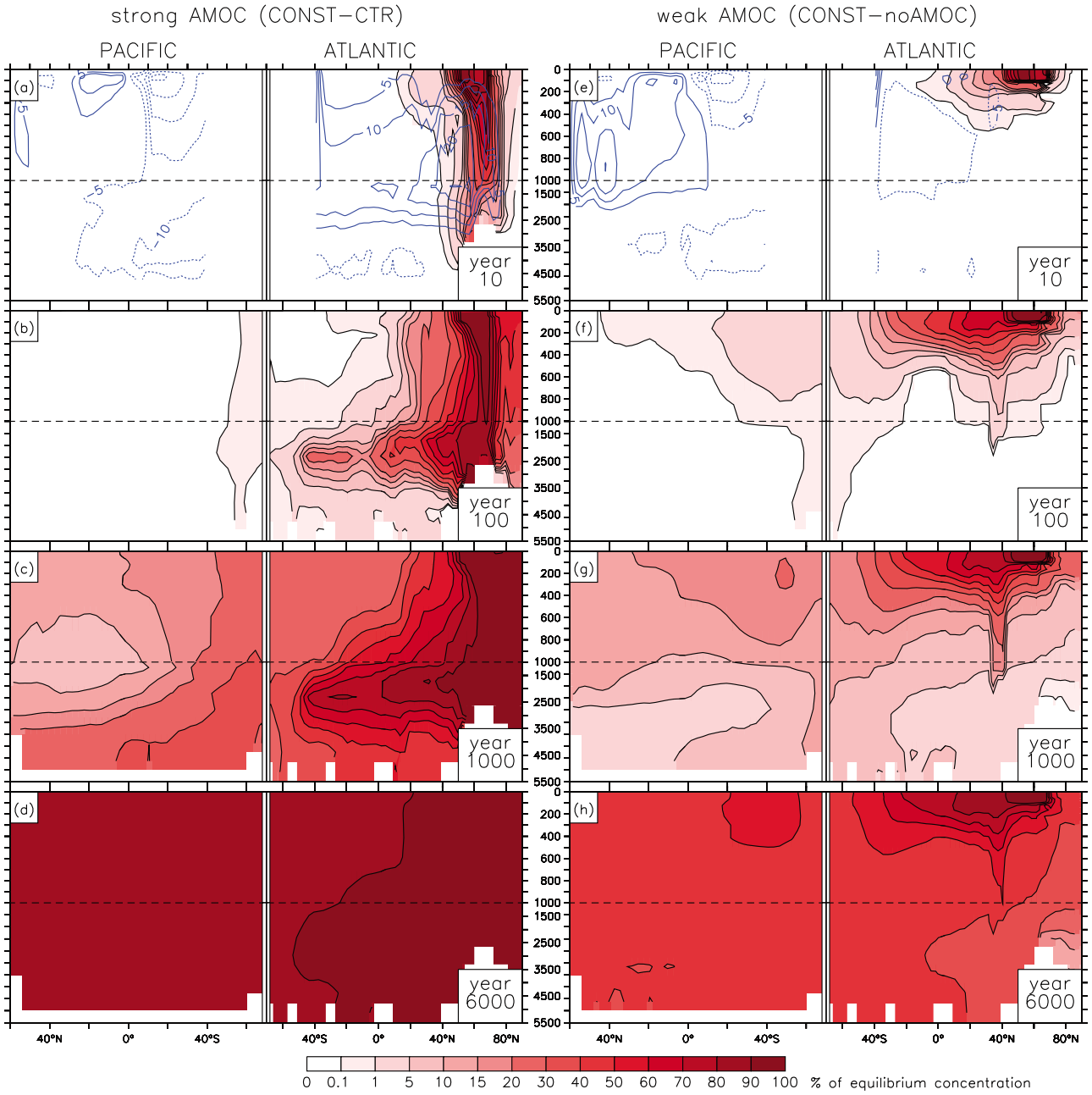

Figure 3. (a–d) Passive tracer concentration for CONST-CTR run in percent of equilibrium concentration zonally averaged for Pacific (left) and Atlantic (right) respectively. Times as indicated in the panels. (e–h) Same as Figures 3a–3d for CONST-noAMOC run. Blue contours in Figures 3a and 3e represent meridional overturning stream functions (Sv) averaged over the entire runs. Please note the non-linear colorscale and the split z-axis.

[25] The development of a PMOC during the AMOC shutdown phase leads to a decoupling of the propagation timescale of our passive tracer from water mass ages in the Pacific below 1,000 m. Figure 5 illustrates that the ratio Γ between δ^{18}O tracer half saturation time (for a North Atlantic deglacial δ^{18}O injection) and a water mass age tracer is significantly larger than one, in the Southern Ocean and the North Pacific, even in the CONST-CTR simulations. During the ~3,000-yearlong AMOC shutdown that is similar to the one reconstructed for H1 [*Bard et al.*, 2000; *Clark et al.*, 2002; *McManus et al.*, 2004] in experiment CONST-FW2ka, also the ratio in the North Atlantic attains values of 2–3. In this case strong ventilation in the North Pacific reduces the water mass age considerably. However, the half saturation time of the δ^{18}O signal in the deep North Pacific increases to up to ~5,000 years, thereby generating a very large North Pacific ratio Γ of 10–30 in the upper 2,000 m. In other words, paleo ventilation age estimates obtained for instance with radio-carbon data, are an unreliable proxy for the time it takes the deglacial δ^{18}O signal to reach the

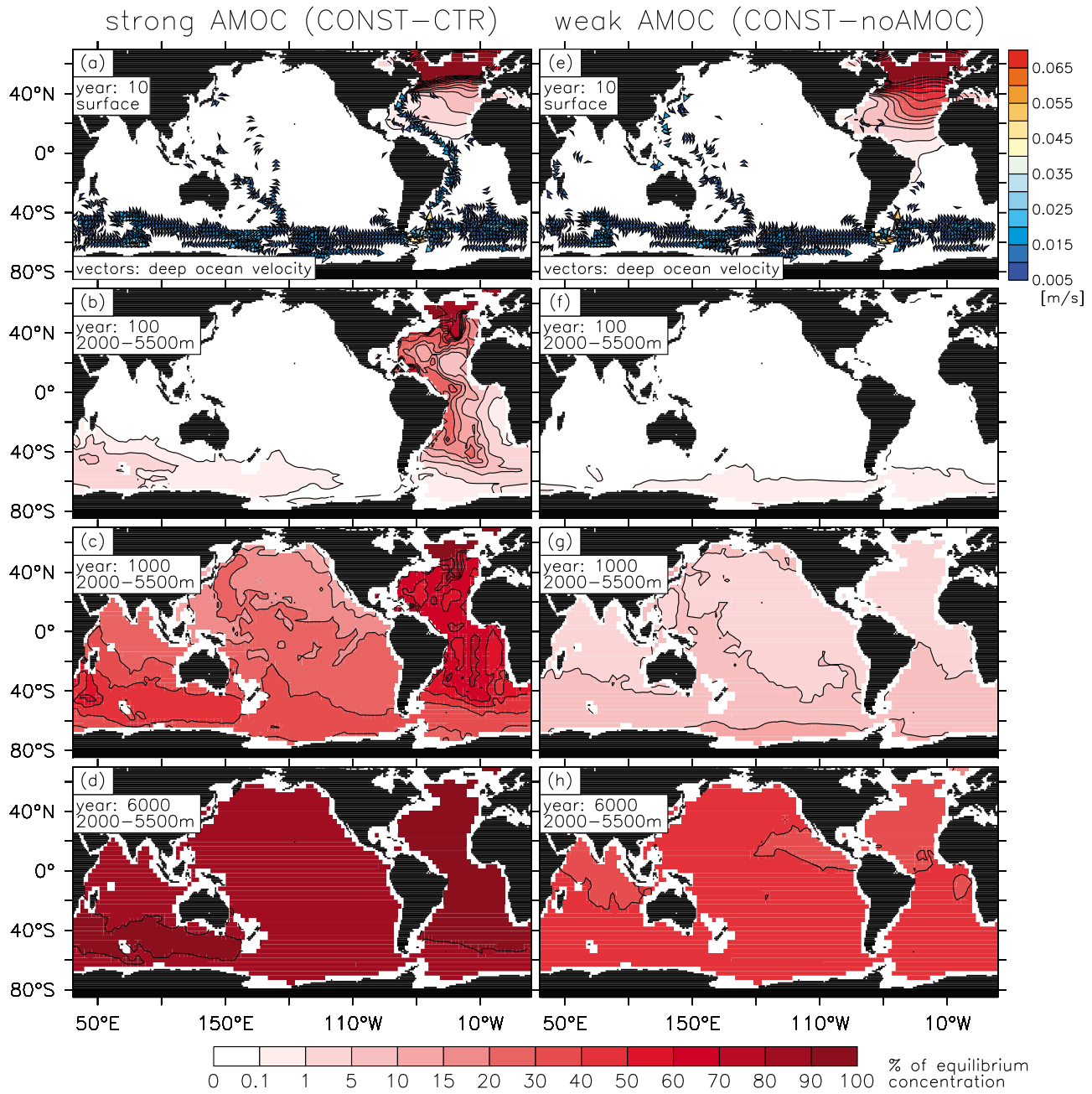

Figure 4. (a–d) Passive tracer concentration for CONST-CTR run in percent of equilibrium concentration for times and depths as indicated in the panels. Vectors in Figure 4a show the mean deep ocean velocity for the model simulation averaged between 2,000 and 5,500 m. Vectors north of 40°N and for velocities <5 mm/s are omitted for clarity. (e–h) Same as Figures 4a–4d for CONST-noAMOC run. Please note the non-linear colorscale for passive tracer concentration.

location of interest. Hence, arguments invoking radiocarbon age constraints in the context of benthic δ^{18}O spreading [*Duplessy et al.*, 1991] have to be revisited, as already pointed out by *Wunsch and Heimbach* [2008] and *Siberlin and Wunsch* [2011].

[26] The experiments described above represent highly idealized scenarios. However, one immediate implication of our results is that in case of a North Atlantic tracer injection the turn-over timescale of the oceans that is often assumed to be in the order of ~1,000–1,500 years [*Duplessy et al.*, 1991] is significantly smaller than the tracer equilibration timescale for a North Atlantic surface tracer injection. Furthermore, we have shown that the latter depends heavily on the state of the large-scale ocean circulation. Our results also imply that a ~3,000-yearlong AMOC weakening during Heinrich event 1 [*Bard et al.*, 2000; *Clark et al.*, 2002; *McManus et al.*, 2004]

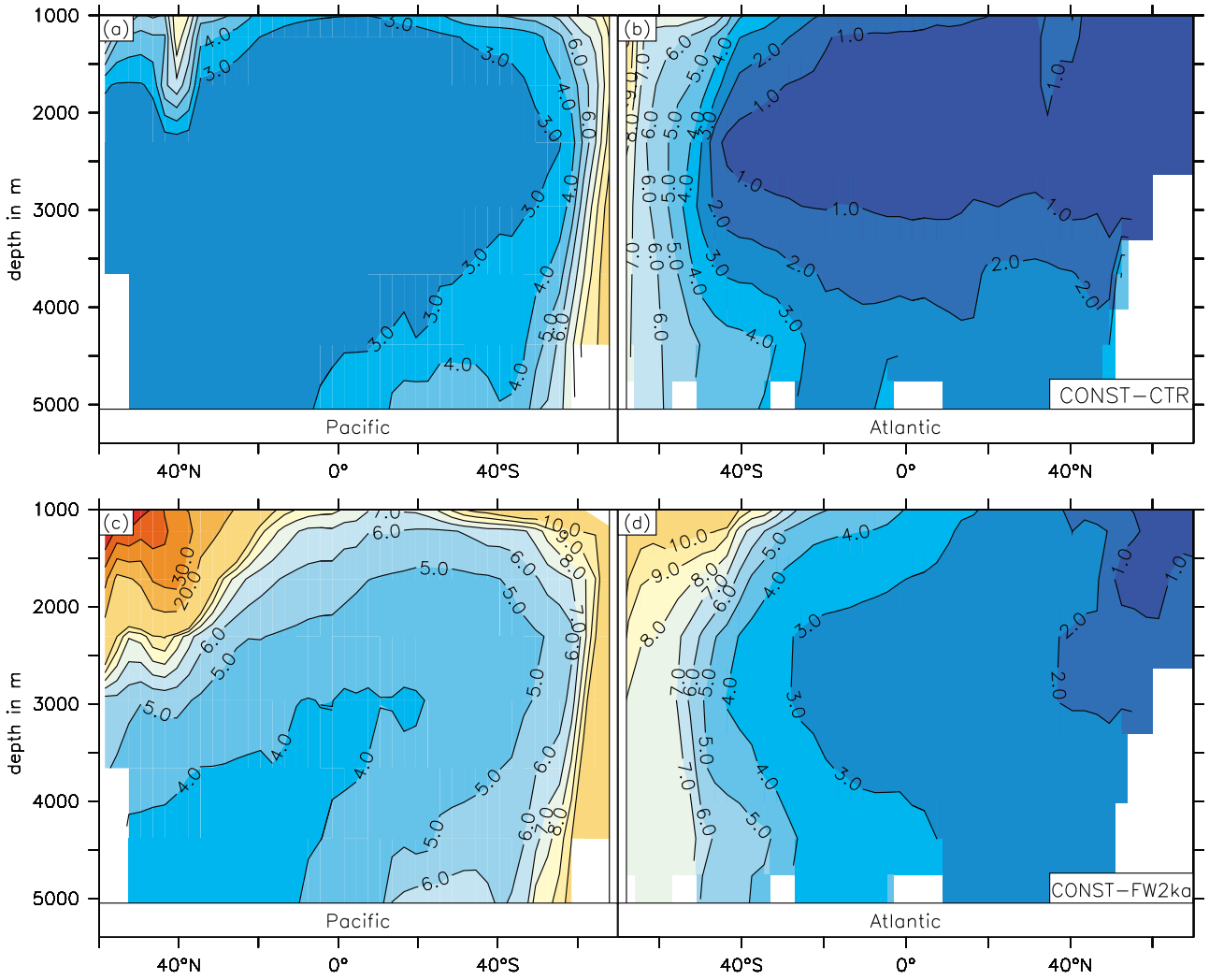

Figure 5. (a) Pacific and (b) Atlantic zonal mean of the ratio of δ^{18}O half saturation time for a North Atlantic injection and the water mass age (derived from a water-age tracer), as simulated by CONST-CTR. (c and d) Same as Figures 5a and 5b, but for experiment CONST-FW2ka averaged for model years 1,800–2,300.

may have caused substantial lags between surface North Atlantic and deep Pacific δ^{18}O reaching up to ~4,000 years.

4.2. Transient Tracer Forcing in the North Atlantic

[27] To elucidate how the time-varying deglacial North Atlantic planktonic δ^{18}O signal is propagated through the ocean under time-varying deglacial freshwater forcing and δ^{18}O, we further study the results of the transient T1-H1 andT1-CTR experiments. Figure 6a reveals that the adopted freshwater forcing generates an AMOC shutdown, that qualitatively resembles the observed evolution of North Atlantic Pa/Th anomalies [*McManus et al.*, 2004] which are believed to be indicative of deep ocean ventilation. Note, however, that given the uncertainties associated with the analysis of Pa/Th data, their robustness is still a matter of debate [*Siddall et al.*, 2007; *Negre et al.*, 2010; *Burke et al.*, 2011].

[28] The resumption of the AMOC coincides with the Bølling Allerød. No attempt was made here to simulate the AMOC weakening during the Younger Dryas around 13–11 ka B.P.

[29] In the control run that uses only the transient δ^{18}O-forcing but no FW-forcing (T1-CTR), the simulated δ^{18}O concentrations in the North Atlantic below 2,000 m (we choose the location of the Iberian Margin core MD99-2334 [*Skinner and Shackleton*, 2005]) show only little phase lag with respect to the surface values driven by the δ^{18}O stack (Figure 6b). However, as a result of the slow propagation, the simulated benthic δ^{18}O does not capture the H1 freshwater peak in the planktonic forcing around 16.5 ka B.P. The heavy smoothing of the planktonic δ^{18}O source signal in deep cores can be described in terms of a convolution of the source function with the Greens-function of the problem [*Wunsch*, 2002]. Hence we conclude that benthic δ^{18}O sea level reconstructions are very likely to miss important millennial-scale and faster variations in deglacial meltwater forcing. The simulated lag between the deep eastern Equatorial Pacific (we have chosen the location of the core TR163-31B [*Skinner and Shackleton*, 2005]) and the deep North Atlantic (location of MD99-2334) amounts to about 1,000 years in T1-CTR (Figure 6b). As a result of a substantial decrease in

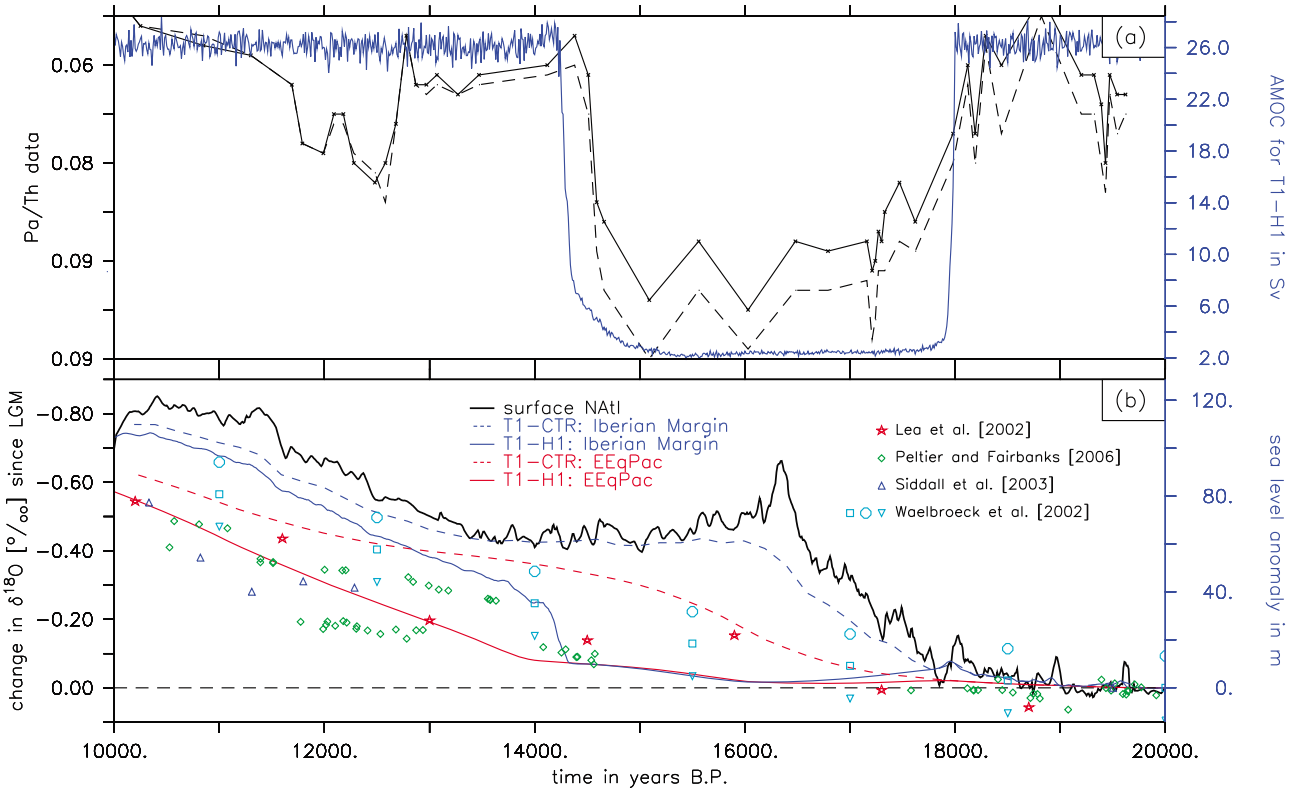

Figure 6. (a) AMOC in Sv for T1-H1 run (blue line) and Pa/Th data (black line) [*McManus et al.*, 2004]. Please note that no attempt was made to simulate the AMOC weakening around 13 ka B.P. The strength of the AMOC is defined by the maximum of the overturning in the Atlantic north of 30°N. (b) Estimates of glacioeustatic sea level anomalies (relative to the LGM) (symbols) from *Lea et al.* [2002], *Peltier and Fairbanks* [2006], *Siddall et al.* [2003], and *Waelbroeck et al.* [2002]. Averaged surface North Atlantic deglacial meltwater forcing (black), simulated Iberian Margin (2,000–4,000 m, blue) and eastern equatorial Pacific (2,000–4,000 m, red) δ^{18}O(x,y,z,t) anomalies (relative to LGM) for TR-CTR (dashed) and TR-H1 (solid).

the strength of the AMOC in T1-H1 the simulated lag between surface forcing in the Atlantic and benthic δ^{18}O values increases to about 2,500–3,000 years. However, the Atlantic-Pacific lag in the benthic signal remains virtually the same.

[30] To further decompose the Iberian margin sediment core δ^{18}O signal into a local glacioeustatic contribution $\delta^{18}O_{sl}(\vec{x},t)$, a temperature contribution $\delta^{18}O_{temp}(\vec{x},t)$ and a water mass contribution $\delta^{18}O_{hydro}(\vec{x},t)$, we subtract the estimates of the local glacioeustatic $\delta^{18}O_{sl}(\vec{x},t)$ (simulated by T1-H1) (Figure 7a, blue line) and the temperature contribution (derived and scaled from the benthic Mg/Ca derived temperature of core MD99-2334 [*Skinner et al.*, 2003; *Skinner and Shackleton*, 2006]) (Figure 7a, purple line) from the benthic δ^{18}O Iberian Margin record (Figure 7a, cyan line). According to our reasoning, the residual (see Figure 7b, black line) captures the δ^{18}O variations due to hydrographic changes and shows a massive intrusion of isotopically heavy waters during Bølling Allerød (BA) and a depletion during Heinrich event 1 and Younger Dryas. This is consistent with the notion of an increased intrusion of Antarctic bottom water (isotopically light in δ^{18}O) during H1, and a replenishment of isotopically heavier Atlantic Deepwater during the BA. An independent confirmation is provided by the benthic δ^{13}C record from the Iberian Margin [*Skinner and Shackleton*, 2004] which reveals isotopically lighter water during Heinrich event 1, reminiscent of Antarctic Bottom Water and a positive anomaly during BA.

[31] For the deep eastern equatorial Pacific core TR163-31B, the decomposition leads to very different results. Overall the magnitudes of the observed benthic δ^{18}O change (Figure 7c, cyan), the simulated deglacial sea level contribution (Figure 7a, blue) and the reconstructed temperature changes (Figure 7a, purple) are smaller than for the North Atlantic. The residual (Figure 7d) shows millennial-scale variability in hydrographic δ^{18}O superimposed onto an overall deglacial trend toward more negative values. A more detailed interpretation of these results in the context of changes in AABW and Glacial Pacific Deep water is beyond the scope of the present study.

[32] Whereas, our approach clearly reveals the state-dependence of the regional $\delta^{18}O'_{sl}(\vec{x},t)$ signal, we also see that both for the Iberian margin core and the deep eastern equatorial Pacific core, its effects are relatively small compared to the massive deglacial changes in $\delta^{18}O_{temp}(\vec{x},t)$ and $\delta^{18}O_{hydro}(\vec{x},t)$, respectively.

5. Discussion and Conclusions

[33] The main findings of our transient experiments reveal that an AMOC weakening such as during Heinrich event 1 cannot create a lead-lag relationship in the benthic δ^{18}O as

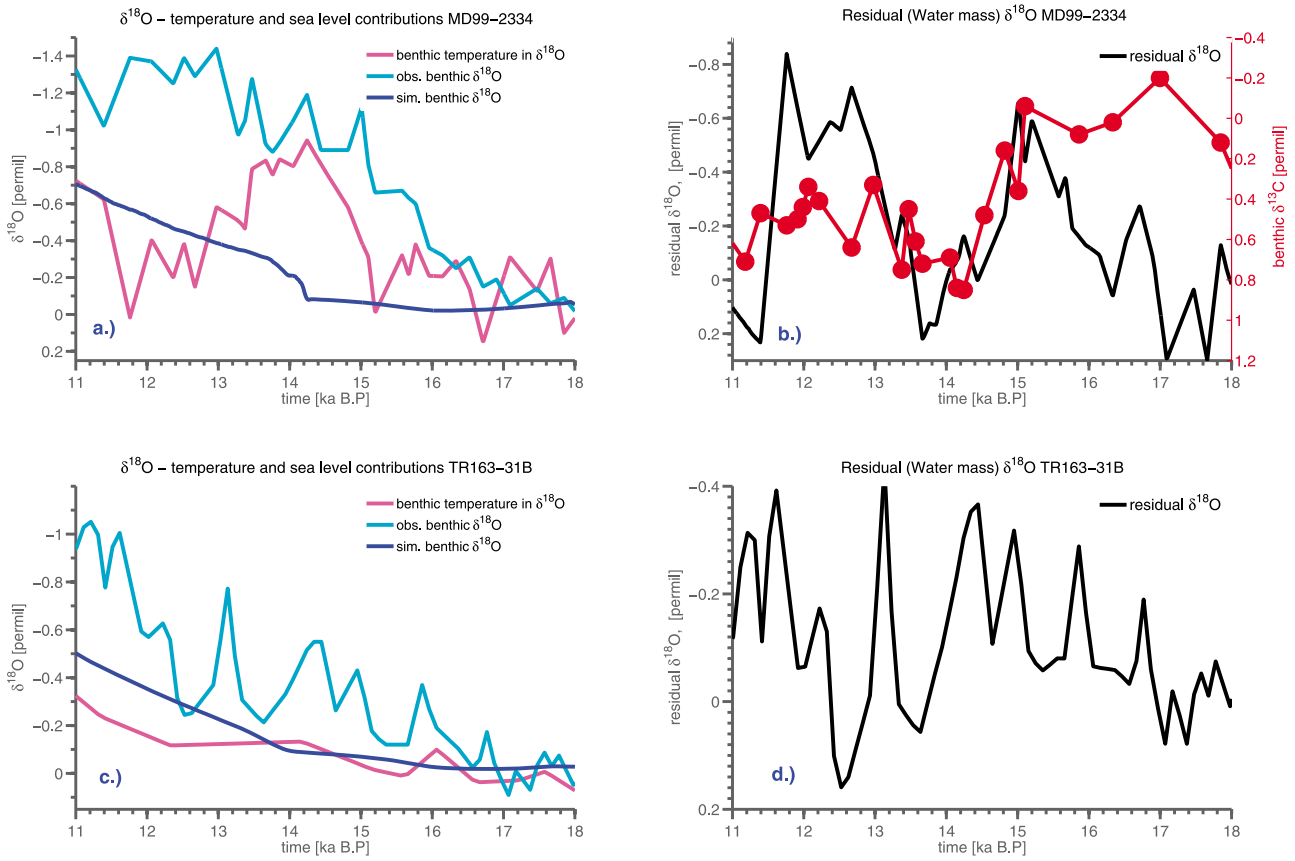

Figure 7. (a) Simulated glacioeustatic benthic δ^{18}O signal for T1-H1 (blue) at the location of MD99-2334 in the northeastern Atlantic and at 3150 m depth, reconstructed benthic δ^{18}O (cyan) from MD99-2334 [*Skinner and Shackleton*, 2004; *Waelbroeck et al.*, 2011], and reconstructed temperature effect on δ^{18}O (purple) obtained from benthic Mg/Ca-temperature data [*Skinner and Shackleton*, 2005] translated to δ^{18}O. All time series are anomalies relative to the LGM. (b) Residual benthic δ^{18}O (black) derived by subtracting the temperature effect and the simulated regional glacioeustatic effect from the observed data, benthic δ^{13}C from *Planulina wuellerstorfi* (red) in MD99-2334 [*Skinner and Shackleton*, 2004]. (c) Same as Figure 7a but for deep eastern equatorial Pacific core TR163-31B [*Skinner and Shackleton*, 2005]. (d) Residual water mass-related benthic δ^{18}O in TR163-31B.

observed by *Skinner and Shackleton* [2005]. However, our results also show that a "sluggish" ocean circulation can create a lag of several thousand years between the (surface) source region of the meltwater-induced δ^{18}O signal and other parts of the oceans. This result further challenges common practices of dating cores using benthic δ^{18}O stacks [*Lisiecki and Raymo*, 2005], at least during times of massive ocean circulation changes, such as glacial terminations. Furthermore, estimates of non-glacioeustatic contributions [*Skinner and Shackleton*, 2005] often rely on the assumption that benthic δ^{18}O stacks represent the actual regional δ^{18}O value due to ice-volume changes. According to our results this assumption needs to be revisited, since the spatiotemporal characteristics of the ice sheet melt signal in benthic δ^{18}O can not be ignored. Figure 8 shows the depth-time evolution of the horizontally averaged error $\Delta = \delta^{18}O(z,t) - \delta^{18}O(t)$ between the horizontally averaged $\delta^{18}O(z,t)$ and the global mean $\delta^{18}O(t)$ (shading) as well as the percentage change relative to the LGM value $\epsilon = \Delta/[\delta^{18}O(t) - \delta^{18}O(t = 20\,\text{ka})] \times 100\%$.

[34] Assuming that the North Atlantic δ^{18}O injection represents the effect of the disintegrating Northern Hemispheric ice sheets, the volume integral of δ^{18}O represents the glacioeustatic sea level component. Figures 8a and 8b displays the regional manifestation of the sea level component in δ^{18}O as a function of depth, time and ocean circulation. We observe that for a weak AMOC (Figure 8b), there is a significant delay of the global deglacial sea level component in δ^{18}O at depths of >2,000 m and an overestimation for depths shallower than 1,000 m. During H1, when the global mean benthic δ^{18}O sea level signal has already decreased by 0.1–0.2 permil (see Figure 6b), the tracer concentrations in TR-H1 at depths below 2000 m have only reached 50% of this value. At the same time the injection of δ^{18}O at the surface leads to temporary vertical deviations from the global mean deglacial signal that attain values of up to 200%. With the recovery of the AMOC around 15 ka B.P. the situation reverses and the deep ocean values are even exceeding the global deglacial signal, whereas the surface values are lagging behind. These results clearly demonstrate that during

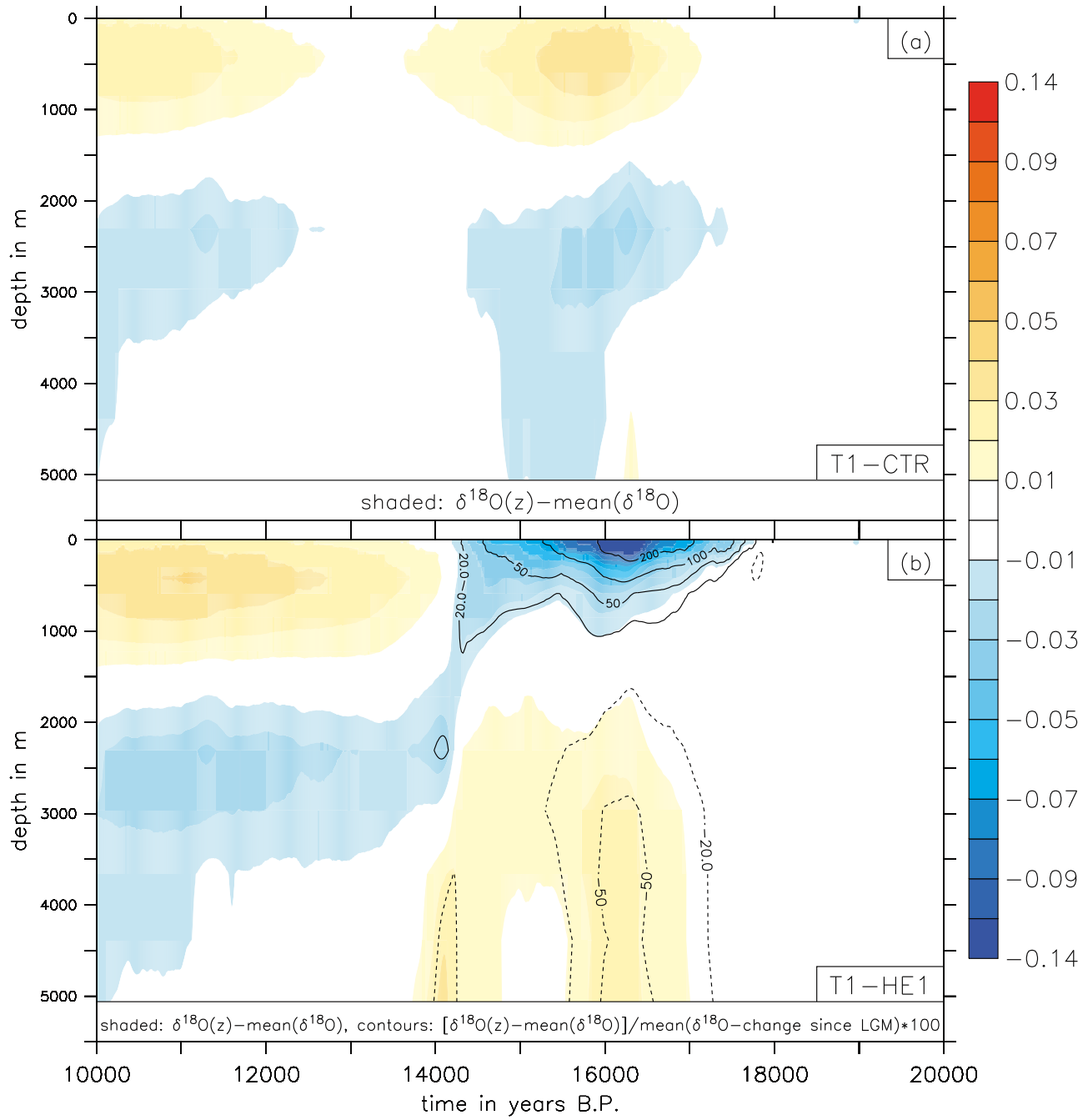

Figure 8. (a) Shading: Hovmöller diagram of the horizontally averaged error [permil] between the δ^{18}O(z,t) and the horizontally and vertically averaged δ^{18}O(t) for T1-CTR. (b) Same as Figure 8a but for T1-H1. Contours: relative error (ϵ) with respect to the horizontally and vertically averaged δ^{18}O(t) change since LGM; $\epsilon = [\delta^{18}\mathrm{O(z,t)}\text{-}\delta^{18}\mathrm{O(t)}]/[\delta^{18}O(t) - \delta^{18}\mathrm{O(LGM)}] \times 100\%$.

periods of large changes of the AMOC, substantial errors can occur in estimating the glacioeustatic signal from benthic δ^{18}O variations.

[35] Our results also demonstrate that ventilation ages or water mass ages should not be confused with the timescale it takes the North Atlantic deglacial δ^{18}O signal to reach a particular location (Figure 5), measured in terms of the half saturation time of a quasi-active tracer, such as δ^{18}O.

[36] Furthermore, the large changes in the propagation pathways that occur in response to the FW forcing in our study (Figures 3 and 4) call for a revision of concepts that heavily rely on the assumption of stationarity of the ocean circulation [*Holzer and Hall*, 2000; *Peacock and Maltrud*, 2006; *Gebbie and Huybers*, 2010; *Gebbie*, 2012] and short ocean 'turn over' timescales [*Duplessy et al.*, 1991] in the context of deglacial climate change and millennial-scale variability associated with Heinrich events and other meltwater pulses. It remains arguable whether TTDs derived from OGCMs run under present-day climatological conditions can be used as a tool to explain the temporal evolution

of paleo-proxies on millennial timescales. However, our results cannot not rule out the possibility that interbasin lags in benthic δ^{18}O are driven by regionally varying surface conditions and their constructive and destructive interference [*Gebbie*, 2012]. Ideally, the two scenarios should be combined to allow for both a regionally varying surface δ^{18}O/FW forcing and an ocean circulation that responds accordingly.

[37] Summarizing, our paper has demonstrated the complexities in interpreting the δ^{18}O of benthic foraminifera in the context of rapidly varying ocean circulations. Our study focuses only on the northern hemispheric source of deglacial δ^{18}O. A more refined hemispheric distribution of the δ^{18}O sources may help to improve our current estimates of $\delta^{18}O'_{sl}$, but such results will still be prone to uncertainties in freshwater forcing originating from the disintegrating glacial ice sheets.

[38] **Acknowledgments.** This work was funded by NSF grant 1010869 and was supported by the Japan Agency for Marine-Earth Science and Technology (JAMSTEC) through its sponsorship of the International Pacific Research Center. The authors would like to thank the two anonymous reviewers and the Editor, Rainer Zahn, for their constructive comments. This is International Pacific Research Center contribution 896 and School of Ocean and Earth Science and Technology contribution 8702.

References

Bard, E., F. Rostek, J.-L. Turon, and S. Gendreau (2000), Hydrological impact of Heinrich Events in the subtropical northeast Atlantic, *Science*, *289*, 1321–1324.

Broecker, W. S., and J. van Donk (1970), Insolation changes, ice volumes, and the O^{18} record in deep-sea cores, *Rev. Geophys.*, *8*, 169–198.

Burke, A., O. Marchal, L. I. Bradtmiller, J. F. McManus, and R. François (2011), Application of an inverse method to interpret $^{231}Pa/^{230}Th$ observations from marine sediments, *Paleoceanography*, *26*, PA1212, doi:10.1029/2010PA002022.

Campin, J. M. (1997), Modélisation tridimensionnelle de la circulation générale océanique lors du dernier maximum glaciaire, PhD thesis, Univ. Catholique de Louvain, Louvain-la-Neuve, Belgium.

Clark, P., N. Pisias, T. Stocker, and A. Weaver (2002), The role of the thermohaline circulation in abrupt climate change, *Nature*, *415*, 863–869.

Decloedt, T., and D. S. Luther (2010), On a simple empirical parameterization of topography-catalyzed diapycnal mixing in the abyssal ocean, *J. Phys. Oceanogr.*, *40*, 487–508.

de Vernal, A., and C. Hillaire-Marcel (2000), Sea-ice cover, sea-surface salinity and halo-/thermocline structure of the northwest North Atlantic: Modern versus full glacial conditions, *Quat. Sci. Rev.*, *19*, 65–85.

Dokken, T. M., and E. Jansen (1999), Rapid changes in the mechanism of ocean convection during the last glacial period, *Nature*, *401*, 458–461.

Dreger, D. (1999), Decadal-to-centennial-scale sediment records of ice advance on the Barents shelf and meltwater discharge into the northeastern Norwegian Sea over the last 40 kyr, PhD thesis, 79 pp., Univ. of Kiel, Kiel, Germany.

Duplessy, J.-C., E. Bard, M. Arnold, N. Shackleton, J. Duprat, and L. Labeyrie (1991), How fast did the ocean-atmosphere system run during the last deglaciation?, *Earth Planet. Sci. Lett.*, *103*(1–4), 27–40, doi:10.1016/0012-821X(91)90147-A.

Elliot, M., L. Labeyrie, and J.-C. Duplessy (2002), Changes in North Atlantic deep-water formation associated with the Dansgaard-Oeschger temperature oscillations (60–10 ka), *Quat. Sci. Rev.*, *21*(10), 1153–1165, doi:10.1016/S0277-3791(01)00137-8.

Emiliani, C. (1966), Paleotemperature analysis of Caribbean cores P6304-8 and P6304-9 and a generalized temperature curve for the past 425,000 years, *J. Geol.*, *74*(2), 109–126.

England, M. (1995), The age of water and ventilation time-scales in a global ocean model, *J. Phys. Oceanogr.*, *25*, 2756–2777.

Friedrich, T., A. Timmermann, T. Decloedt, D. S. Luther, and A. Mouchet (2011), The effect of topography-enhanced diapycnal mixing on ocean and atmospheric circulation and marine biogeochemistry, *Ocean Modell.*, *39*(3–4), 262–274, doi:10.1016/j.ocemod.2011.04.012.

Gebbie, G. (2012), Tracer transport timescales and the observed Atlantic-Pacific lag in the timing of the last termination, *Paleoceanography*, doi:10.1029/2011PA002273, in press.

Gebbie, G., and P. Huybers (2010), Total matrix intercomparison: A method for determining the geometry of water-mass pathways, *J. Phys. Oceanogr.*, *40*, 1710–1728.

Gebbie, G., and P. Huybers (2011), How is the ocean filled?, *Geophys. Res. Lett.*, *38*, L06604, doi:10.1029/2011GL046769.

Goosse, H., E. Deleersnijder, T. Fichefet, and M. England (1999), Sensitivity of a global coupled ocean-sea ice model to the parameterization of vertical mixing, *J. Geophys. Res.*, *104*(C6), 13,681–13,695.

Goosse, H., et al. (2010), Description of the Earth system model of intermediate complexity LOVECLIM version 1.2, *Geophys. Model Dev.*, *3*, 603–633.

Hemming, S. R. (2004), Heinrich events: Massive late Pleistocene detritus layers of the North Atlantic and their global climate imprint, *Rev. Geophys.*, *42*, RG1005, doi:10.1029/2003RG000128.

Holzer, M., and T. M. Hall (2000), Transit-time and tracer-age distributions in geophysical flows, *J. Atmos. Sci.*, *57*, 3539–3558.

Hu, A., G. A. Meehl, B. L. Otto-Bliesner, C. Waelbroeck, W. Han, M.-F. Loutre, K. Lambeck, J. X. Mitrovica, and N. Rosenbloom (2010), Influence of Bering Strait flow and North Atlantic circulation on glacial sea-level changes, *Nat. Geosci.*, *3*, 118–121.

Justino, F., A. Timmermann, U. Merkel, and E. Souza (2005), Synoptic reorganization of atmospheric flow during the last glacial maximum, *J. Clim.*, *18*(15), 2826–2846.

Keigwin, L. D., J. P. Sachs, Y. Rosenthal, and E. A. Boyle (2005), The 8200 year B.P. event in the slope water system, western subpolar North Atlantic, *Paleoceanography*, *20*, PA2003, doi:10.1029/2004PA001074.

Lambeck, K., and J. Chappell (2001), Sea level change through the last glacial cycle, *Science*, *292*, 679–686.

Lea, D. W., P. A. Martin, D. K. Pak, and H. J. Spero (2002), Reconstructing a 350 ky history of sea level using planktonic Mg/Ca and oxygen isotope records from a Cocos Ridge core, *Quat. Sci. Rev.*, *21*(1–3), 283–293, doi:10.1016/S0277-3791(01)00081-6.

LeGrande, A. N., and G. A. Schmidt (2006), Global gridded data set of the oxygen isotopic composition in seawater, *Geophys. Res. Lett.*, *33*, L12604, doi:10.1029/2006GL026011.

Lisiecki, L. E., and M. E. Raymo (2005), A Pliocene-Pleistocene stack of 57 globally distributed benthic δ^{18}O records, *Paleoceanography*, *20*, PA1003, doi:10.1029/2004PA001071.

Lisiecki, L. E., and M. E. Raymo (2009), Diachronous benthic δ^{18}O responses during late Pleistocene terminations, *Paleoceanography*, *24*, PA3210, doi:10.1029/2009PA001732.

McManus, J. F., R. Francois, J. M. Gherardi, L. D. Keigwin, and S. Brown-Leger (2004), Collapse and rapid resumption of Atlantic meridional circulation linked to deglacial climate changes, *Nature*, *428*, 834–837.

Menviel, L., A. Timmermann, A. Mouchet, and O. Timm (2008), Meridional reorganization of marine and terrestrial productivity during Heinrich events, *Paleoceanography*, *23*, PA1203, doi:10.1029/2007PA001445.

Negre, C., R. Zahn, A. L. Thomas, P. Masqué, G. M. Henderson, G. Martínez-Méndez, I. R. Hall, and J. L. Mas (2010), Reversed flow of Atlantic deep water during the Last Glacial Maximum, *Nature*, *468*, 84–88, doi:10.1038/nature09508.

Okazaki, Y., A. Timmermann, L. Menviel, N. Harada, A. Abe-Ouchi, M. O. Chikamoto, A. Mouchet, and H. Asahi (2010), Deep water formation in the North Pacific during the Last Glacial Termination, *Science*, *329*, 200–204.

Peacock, S., and M. Maltrud (2006), Transit-time distributions in a global ocean model, *J. Phys. Oceanogr.*, *36*, 474–495.

Peltier, W., and R. Fairbanks (2006), Global glacial ice volume and Last Glacial Maximum duration from an extended Barbados sea level record, *Quat. Sci. Rev.*, *25*(23–24), 3322–3337, doi:10.1016/j.quascirev.2006.04.010.

Polzin, K., J. M. Toole, and R. W. Schmitt (1995), Finescale parameterizations of turbulent dissipation, *J. Phys. Oceanogr.*, *25*, 306–328.

Renssen, H., H. Goosse, and T. Fichefet (2002), Modeling the effect of freshwater pulses on the early Holocene climate: The influence of high-frequency climate variability, *Paleoceanography*, *17*(2), 1020, doi:10.1029/2001PA000649.

Rood, R. B. (1987), Numerical advection algorithms and their role in atmospheric transport and chemistry models, *Rev. Geophys.*, *25*(1), 71–100, doi:10.1029/RG025i001p00071.

Shackleton, N. J. (1967), Oxygen isotope analysis and pleistocene temperature reassessed, *Nature*, *215*, 15–17.

Shackleton, N. J., and N. D. Opdyke (1973), Oxygen isotope and palaeomagnetic stratigraphy of Equatorial Pacific core V28-238: Oxygen isotope temperatures and ice volumes on a 10^5 year and 10^6 year scale, *Quat. Res.*, *3*(1), 39–55, doi:10.1016/0033-5894(73)90052-5.

Siberlin, C., and C. Wunsch (2011), Oceanic tracer and proxy time scales revisited, *Clim. Past*, *7*(1), 27–39, doi:10.5194/cp-7-27-2011.

Siddall, M., E. J. Rohling, A. Almogi-Labin, C. Hemleben, D. Meischner, I. Schmelzer, and D. A. Smeed (2003), Sea-level fluctuations during the last glacial cycle, *Nature*, *423*, 853–858.

Siddall, M., T. F. Stocker, G. M. Henderson, F. Joos, M. Frank, N. R. Edwards, S. P. Ritz, and S. A. Müller (2007), Modeling the relationship between ^{231}Pa/^{230}Th distribution in North Atlantic sediment and Atlantic meridional overturning circulation, *Paleoceanography*, *22*, PA2214, doi:10.1029/2006PA001358.

Skinner, L. C., and N. J. Shackleton (2004), Rapid transient changes in Northeast Atlantic deep-water ventilation-age across Termination I, *Paleoceanography*, *19*, PA2005, doi:10.1029/2003PA000983.

Skinner, L. C., and N. J. Shackleton (2005), An Atlantic lead over Pacific deep-water change across Termination I: Implications for the application of the marine isotope stage stratigraphy, *Quat. Sci. Rev.*, *24*, 571–580.

Skinner, L. C., and N. J. Shackleton (2006), Deconstructing Terminations I and II: Revisiting the glacioeustatic paradigm based on deep-water temperature estimates, *Quat. Sci. Rev.*, *25*, 3312–3321.

Skinner, L. C., N. J. Shackleton, and H. Elderfield (2003), Millennial-scale variability of deep-water temperature and $\delta^{18}O_{dw}$ indicating deep water source variations in the Northeast Atlantic, 0–34 cal. ka. BP, *Geochem. Geophys. Geosyst.*, *4*(12), 1098, doi:10.1029/2003GC000585.

Smith, W. H. F., and D. T. Sandwell (1997), Global sea floor topography from satellite altimetry and ship depth soundings, *Science*, *277*, 1956–1962.

Vidal, L., L. Labeyrie, E. Cortijo, M. Arnold, J.-C. Duplessy, E. Michel, S. Becqué, and T. van Weering (1997), Evidence for changes in the North Atlantic Deep Water linked to meltwater surges during the Heinrich events, *Earth Planet. Sci. Lett.*, *146*(1–2), 13–27, doi:10.1016/S0012-821X(96)00192-6.

Waelbroeck, C., L. Labeyrie, E. Michel, J.-C. Duplessy, J. McManus, K. Lambeck, E. Balbon, and M. Labracherie (2002), Sea-level and deep water temperature changes derived from benthic foraminifera isotopic records, *Quat. Sci. Rev.*, *21*(1.–3), 295–305, doi:10.1016/S0277-3791(01)00101-9.

Waelbroeck, C., L. C. Skinner, L. Labeyrie, J.-C. Duplessy, E. Michel, N. V. Riveiros, J. Gherardi, and F. Dewilde (2011), The timing of deglacial circulation changes in the Atlantic, *Paleoceanography*, *26*, PA3213, doi:10.1029/2010PA002007.

Wunsch, C. (2002), Oceanic age and transient tracers: Analytical and numerical solutions, *J. Geophys. Res.*, *107*(C6), 3048, doi:10.1029/2001JC000797.

Wunsch, C., and P. Heimbach (2008), How long to oceanic tracer and proxy equilibrium, *Quat. Sci. Rev.*, *27*, 637–651.